

The abundance of compact quiescent galaxies since $z \sim 0.6$

Aldée Charbonnier^{1*}, Marc Huertas-Company^{2,3}, Thiago S. Gonçalves¹, Kevin Bundy⁴, Karín Menéndez-Delmestre¹, Emmanuel Galliano¹, Bruno Moraes⁵, Maria E. S. Pereira⁶, Martín Makler⁶, Thomas Erben⁷, Hendrik Hildebrandt⁷, Huan-Yuan Shan⁸, G. B. Caminha⁹, Marco Grossi¹, Laurie Riguccini¹

¹ Observatório do Valongo, Universidade Federal do Rio de Janeiro, Ladeira Pedro Antonio 43, Saúde, Rio de Janeiro, RJ, CEP 20080-090, Brazil

² LERMA, Observatoire de Paris, CNRS, Université Paris Diderot, Paris Sciences et Lettres (PSL) Research University, Université Paris Sorbonne Cité, 61 Avenue de l'Observatoire, F-75014 Paris, France

³ Department of Physics and Astronomy, University of Pennsylvania, Philadelphia, PA 19104, USA

⁴ Kavli Institute for the Physics and Mathematics of the Universe (WPI), Todai Institutes for Advanced Study the University of Tokyo, Kashiwa, 277-8582, Japan

⁵ Dept. of Physics and Astronomy, University College London, London, WC1E 6BT, UK

⁶ Centro Brasileiro de Pesquisas Físicas, Rua Dr. Xavier Sigaud 150, CEP 22290-180, Rio de Janeiro, RJ, Brazil

⁷ Argelander-Institut für Astronomie, Auf dem Hügel 71, D-53121 Bonn, Germany

⁸ Laboratoire d'astrophysique (LASTRO), Ecole Polytechnique Fédérale de Lausanne (EPFL), Observatoire de Sauverny, CH-1290 Versoix, Switzerland

⁹ Dipartimento di Fisica e Scienze della Terra, Università degli Studi di Ferrara, Via Saragat 1, I-44122 Ferrara, Italy

Accepted XXX. Received YYY; in original form ZZZ

ABSTRACT

The evolution of high-redshift quiescent massive compact galaxies is still debated. Do these galaxies grow to match the local early-type mass-size relation without significant stellar mass growth? or, do they remain as relics of the past at lower redshifts? Looking for compact galaxies at intermediate redshifts might provide additional clues to answer these questions. We quantify the number density of compact massive ($M_\star > 5 \times 10^{10} M_\odot$) galaxies at intermediate redshifts ($0.2 < z < 0.6$) in the equatorial SDSS Stripe 82 region (~ 250 sq. degrees). This volume allows to decrease the effect of cosmic variance. Structural parameters are obtained in the i-band using the CFHT Stripe 82 (CS82) survey with an exquisite median seeing of $\sim 0''.6$. We explore a variety of definitions of compactness present in the literature. We find that the absolute number of compact galaxies is very dependent on the adopted definition, and can change up to a factor of > 10 . However, we systematically measure a factor of ~ 5 more compacts at the same redshift than what was previously reported on smaller fields with HST imaging, more affected by cosmic variance. This means that the decrease in number density from $z \sim 1.5$ to $z \sim 0.2$ might be only of a factor of $\sim 2 - 5$, significantly smaller than what previously reported: this supports progenitor bias as the main contributor to the size evolution. This decrease is roughly compatible with the predictions from recent numerical simulations. Only extreme compact galaxies ($R_{\text{eff}} < 1.5 \times (M_\star/10^{11} M_\odot)^{0.75}$ and $M_\star > 10^{10.7} M_\odot$) seem to drop in number by a factor of ~ 20 and therefore probably experience a noticeable size evolution.

Key words: galaxies: structure - galaxies: formation - galaxies: evolution - galaxies: ellipticals and lenticulars, cD - catalogues - surveys

1 INTRODUCTION

How galaxies form and evolve through cosmic time is one of the key questions of modern astronomy. In the context of hierarchical formation of structures in a cold

* E-mail: charbonnier@astro.ufrj.br

dark-matter universe, less massive dark matter haloes formed first, and then accreted to form more massive ones (e.g., [Diemand & Moore 2011](#)). The star formation activity, however, is not simply proportional to the halo mass (e.g., [Somerville & Davé 2015](#)) nor constant over cosmic times ([Madau et al. 1998](#); [Madau & Dickinson 2014](#)). Hydro-cosmological simulations predict that massive galaxies tend to quench their star formation earlier and faster than less massive ones ([Zolotov et al. 2015](#)). Studying Sloan Digital Sky Survey (SDSS, [York et al. 2000](#)) massive galaxies, [Citro et al. \(2016\)](#) show that early-type ones are following an anti-hierarchical evolution (downsizing), i.e. massive galaxies are older and quench earlier. The star formation history of the most massive galaxies reveals that they should have been formed by a vigorous star formation event, and be already compact at $z \sim 2 - 3$. An important population of passively evolving massive galaxies is found to be already in place at $z \sim 2$ when the universe was only ~ 3 Gyrs old ([Cimatti et al. 2004](#); [Daddi et al. 2005](#); [Trujillo et al. 2006](#); [Damjanov et al. 2009](#); [Whitaker et al. 2012](#); [Cassata et al. 2013](#); [Huertas-Company et al. 2013, 2015](#)). This population of massive quiescent galaxies observed at high redshifts shows evidence of being 3 to 5 times more compact than its local counterpart ([Daddi et al. 2005](#); [Trujillo et al. 2006](#); [Longhetti et al. 2007](#); [Cimatti et al. 2008](#); [van Dokkum et al. 2008, 2010](#); [Damjanov et al. 2009, 2011](#); [Newman et al. 2010](#); [Bruce et al. 2012](#); [Ryan et al. 2012](#); [Cassata et al. 2013](#); [van der Wel et al. 2014](#)) and is commonly referred to as ‘red-nuggets’.

It remains to be understood how these massive compact galaxies formed: what are their star-forming progenitors and what are the quenching processes involved to turn them into quiescent galaxies. Comparing the number density, stellar mass and size of the population of submillimeter galaxies (SMG) at high redshifts ($z \gtrsim 3$) and of the population of compact massive quiescent galaxies at $z \sim 2$ in the COSMOS field, [Toft et al. \(2014\)](#) have proposed a direct evolutionary connection between these two extreme galaxy types. Some of the SMGs in the process of quenching could be the ones observed by [Barro et al. \(2013\)](#) and [van Dokkum et al. \(2015\)](#) who have identified star-forming progenitors at high redshifts ($z > 2$) in the CANDELS fields that have similar sizes (~ 1 kpc), masses ($\sim 10^{11} M_{\odot}$) and number densities to the quiescent compact galaxies. Measuring star formation rates and gas content of their star-forming candidates, they underline the presence of a gas disc in the potential progenitors with sizes ranging from ~ 0.2 to 10 kpc. One might then expect a compaction process associated with a quenching episode ([Dekel & Burkert 2014](#); [Zolotov et al. 2015](#)). [Williams et al. \(2015\)](#) and [van Dokkum et al. \(2015\)](#) propose a model in which the more compact the star-forming massive galaxies become, the higher is the probability of them being quenched. According to [Franx et al. \(2008\)](#) the likelihood of quenching increases as the velocity dispersion reaches a particular threshold, $\sigma_q = 225 \text{ km s}^{-1}$ (which is equivalent to saying that the specific star-formation rate correlates with the compactness). Environmental quenching ([Peng et al. 2010](#)) may also be in play. Although there is no consensus regarding the quenching mechanism, we note that [Barro et al. \(2013\)](#), [Förster Schreiber et al. \(2014\)](#) and [van Dokkum et al. \(2015\)](#) find that about half of the star-forming progenitors host active galactic nuclei (AGNs).

However there is yet no direct evidence that the AGN is able to drive away the gas by itself ([Zolotov et al. 2015](#)). Alternative models suggest that the origin of compact galaxies and subsequent size evolution might simply be a consequence of the size evolution of star-forming galaxies coupled with progenitor bias effects (e.g., [Carollo et al. 2013](#); [Lilly & Carollo 2016](#)).

Cosmological hydrodynamic simulations may help understand the evolution and formation of these compact massive galaxies. They are taking into account a number of physical processes (e.g., gravity, hydrodynamics, gas cooling, star formation, stellar evolution, supernova and black hole feedback) and are currently able to reproduce the observed properties of galaxy populations thanks to the use of subgrid models for feedback processes (e.g., EAGLE, [Schaye et al. 2015](#) and ILLUSTRIS, [Vogelsberger et al. 2014](#)). Compact massive quiescent galaxies have indeed been identified in simulations at high redshifts ([Wellons et al. 2015](#); [Zolotov et al. 2015](#); [Furlong et al. 2015](#)), allowing us to trace back their formation history. [Zolotov et al. \(2015\)](#) find that the compaction of star-forming discs has to be driven at a rate faster than the star formation rate. The compaction might be due to mergers (both minor and major) in concert with violent disc instabilities (e.g., [Dekel & Burkert 2014](#)). The onset of quenching happens when the galaxy is at its maximum compactness, due to gas depletion. Simulations show therefore that very compact passive galaxies are formed at high redshifts through dissipative process associated with gas inflow into the galaxy central region. As the efficiency of the quenching and compaction processes are correlated with the abundance of cold dense gas in the universe, the production of compact massive quiescent galaxies is expected to decrease with cosmic time. An alternative scenario to explain the shut-down of the star formation invokes the mechanism of ‘halo quenching’ (e.g., [Zu & Mandelbaum 2016](#)), in which the mass of the dark matter halo is the main driver for triggering the quenching. However, it seems that the galaxy compactness is playing a non-negligible role for satellite galaxy quenching ([Woo et al. 2015](#)).

Both observations (e.g., [van der Wel et al. 2014](#)) and cosmological hydrodynamic simulations (e.g., [Wellons et al. 2016](#)) agree on the fact that massive early-type galaxies are smaller in median size at higher redshifts. This is partly due to the so-called progenitor bias, as star-forming galaxies have larger sizes at later times ([Mo et al. 1998](#)). An intrinsic growth of individual galaxies is expected and observed in numerical simulations, due e.g., to: (i) radial migration of stars, (ii) addition of mass to the outer region by mergers or accretion, and (iii) renewed star formation at larger radius. These channels of evolution might conduct the original compact massive quiescent galaxies to become the bulges of local galaxies ([Graham et al. 2015](#); [de la Rosa et al. 2016](#)). These processes are however stochastic: one expects to see the numerical density of compact massive quiescent galaxies decreasing with redshift, leaving some relic candidates untouched. [Wellons et al. \(2016\)](#) and [Furlong et al. \(2015\)](#) have studied the evolution of the population of massive compact quiescent galaxies since high redshift using respectively the ILLUSTRIS and the EAGLE simulations. Compact massive galaxies undergo a variety of processes: [Furlong et al. \(2015\)](#) show that among the original population of compact massive and passive galaxies at $z = 2, 15$

percent remain central cores, 25 percent become satellites, and 60 percent have merged with more massive systems at low redshifts. On their side, Wellons et al. (2016) observe that 14 percent were consumed and accreted by more massive galaxies, 6 percent experienced a major merger event and are partially disrupted, 49 percent remained as the core of a more massive descendant, and 31 percent remained untouched. The growth in size of galaxies with cosmic times is accompanied by a growth in mass that is dominated by ex-situ stars. Wellons et al. (2016) underline that even the undisturbed compact massive sample grows in mass and size. They also confirm the result obtained by Oser et al. (2012), showing that the dominant accretion mode for simulated massive galaxies from $z \sim 2$ to present time is minor mergers with a mass-weighted mass ratio of 1:5. Despite the mean growth in size and mass of the high redshift population of massive compact quiescent galaxies, candidates that did not yet accrete large numbers of external stars and remained compact are expected to be found in the local universe.

The current picture of (and search for) compact massive quiescent galaxies in the local universe is quite unclear. Depending on the definition of compactness and on the nature of the dataset, results are dramatically different. Trujillo et al. (2009) find almost no candidates using the SDSS DR6 NYU value-added galaxy catalogue (NYU VAGC, $z < 0.2$), where they classify 0.03 percent of the population of massive ellipticals as relics. Valentinuzzi et al. (2010a) find, in turn, a large sample in the Wide-field Nearby Galaxy-cluster Survey ($0.04 < z < 0.07$) where 22 percent of the cluster members with masses in the interval $3 \times 10^{10} < M_*/M_\odot < 4 \times 10^{11}$ are red nugget candidates. Taylor et al. (2010) look at the spectroscopic sample of SDSS DR7 and conclude about the dearth of massive quiescent galaxies as compact as at high redshifts in the local universe ($0.066 < z < 0.12$). Adopting the same definition for compact relics as Valentinuzzi et al. (2010a), Poggianti et al. (2013) look for candidates in the field in the context of the Padova-Millennium Galaxy and Group Catalogue ($0.03 < z < 0.11$), and find three times less compact galaxies in the field than in cluster environment. Trujillo et al. (2014) identify a nearby galaxy, NGC 1277, as being one representative of the massive compact relics, with a mass of $1.2 \pm 0.4 \times 10^{11} M_\odot$ and a mean age of 12 Gyr. Based on the same catalogue as Trujillo et al. (2009) but defining differently the compact relics, Peralta de Arriba et al. (2016) find that galaxy clusters might be the preferred environments to find compact relics.

Putting together the set of consistent observations at high redshifts with the discrepant ones locally calls for an analysis based on an intermediate redshift sample, as well as a common definition of the so-called local red nuggets. Such an analysis would provide insights to the evolution processes of the compact massive quiescent galaxy population over cosmic times. The main challenge of intermediate redshift studies is the chosen compromise between the area surveyed and the quality of the images, respectively to have enough statistics and to be able to disentangle stars from compact galaxies. Space based surveys sample limited volumes but benefit from exquisite image resolution, whereas ground based surveys can probe larger volumes but suffer from observational seeing limitations. Recent works using

HST performances found candidates for compact massive quiescent galaxies at intermediate redshifts in the COSMOS field (Carollo et al. 2013; Damjanov et al. 2015) and in the ESO Distant Clusters Survey (Valentinuzzi et al. 2010b). Concerning ground based images, Damjanov et al. (2013) confirmed that non resolved galaxies of SDSS that are identified by their spectra present properties of compact quiescent candidates. Damjanov et al. (2014) proposed a similar approach based on Baryon Oscillation Spectroscopic Survey (BOSS, Eisenstein et al. 2011) data. They were able to derive the density evolution of compact massive candidates at intermediate redshifts, however still with large error bars. A recent analysis made use of the first and second releases of the ESO Public optical Kilo Degree Survey (KiDS) that covers a region of 156 deg^2 in four bands Tortora et al. (2016). Applying similar definitions as in Trujillo et al. (2009), they find a population of compact relic candidates at intermediate redshifts, that seems to stay constant towards lower redshifts within the error bars, however they do not observe any candidates at $z < 0.2$, arguing that it might be due to environment effects.

In the present analysis we look for compact massive quiescent galaxies at intermediate redshifts (from $z = 0.2$ to $z = 0.6$) in the so-called Stripe 82 region. Thanks to uniform, deep, multiwavelength and weak lensing quality data over this large equatorial stripe, we are currently in a privileged position to look for the population of compact candidates. In this work, we adopt a spatially flat cosmological model with $\Omega_M = 0.3$, $\Omega_\Lambda = 0.7$ and $H_0 = 70 \text{ km s}^{-1} \text{ Mpc}^{-1}$. Magnitudes are quoted in the AB system.

2 IDENTIFYING COMPACT CANDIDATES IN STRIPE 82

The so-called Stripe 82 is an equatorial stripe of $\sim 250 \text{ deg}^2$ in the southern Galactic cap. It has been observed by the SDSS repeatedly as part of a supernova survey (e.g., Abazajian et al. 2009), reaching deep magnitudes with a uniform coverage in the *ugriz* optical bands ($i \sim 24.3$ for point like sources at 3σ , Annis et al. 2014; Jiang et al. 2014; Fliri & Trujillo 2016). Following these observations, the field has benefited from a coverage from radio wavelengths to X-rays and thus has become a favourite field for large-scale multiwavelength studies. We list here part of Stripe 82 observations to give an idea of the continuous inflow of new data: deep radio data by the (Karl G. Jansky) Very Large Array (VLA Heywood et al. 2016), microwave from the Atacama Cosmology Telescope (ACT, Swetz et al. 2011), submillimeter from the Herschel satellite (Viero et al. 2014), infrared (IR) from the Spitzer-IRAC instrument (Papovich et al. 2016; Timlin et al. 2016), near-infrared (NIR) from the Wide-Field Infrared Survey Explorer (WISE, Wright et al. 2010), the UKIRT Infrared Deep Sky Survey (UKIDSS, Lawrence et al. 2007) and from a joint VISTA-CFHT survey (Geach et al in prep), *i*-band CFHT data (Kneib et al in prep), X-rays Chandra and XMM-Newton data (LaMassa et al. 2013; Rosen et al. 2016). In terms of spectroscopy, Stripe 82 has been targeted by various surveys, including the SDSS-III Baryon Oscillation Spectroscopic Survey (BOSS, Dawson et al. 2013), the WiggleZ Dark Energy Survey (Drinkwater et al. 2010), the Deep extra-

galactic Evolutionary Probe (DEEP2, [Weiner et al. 2005](#)) and the VIMOS VLT Deep Survey (VVDS [Garilli et al. 2008](#)). Being observable from both south and north hemisphere, this area is becoming a preferred field for calibration purposes of large photometric surveys like the Dark Energy Survey ([Dark Energy Survey Collaboration et al. 2016](#)) and the Large Synoptic Survey Telescope project ([LSST Science Collaboration et al. 2009](#)).

2.1 Datasets and catalogues

Different photometric redshift estimators have been applied to SDSS-Stripe 82 catalogues. [Bundy et al. \(2015\)](#) find that the best performances are obtained both using the red-sequence Matched-filter Probabilistic Percolation algorithm (redMaPPer, [Rykoff et al. 2014](#)), and a neural network approach as done by [Reis et al. \(2012\)](#) with ANNz ([Collister & Lahav 2004](#)). When photo-z's are not available from these catalogues, EAZY (for Easy and Accurate Redshifts from Yale, [Brammer et al. 2008](#)) estimates are used. The details of the photo-z catalogue are explained in [Bundy et al. \(2015\)](#). We give preference to spectroscopic over photometric redshift when available.

In the NIR, UKIDSS ([Lawrence et al. 2007](#)) have targeted Stripe 82 region in *YJHK* bands, reaching $Y \sim 20$. Based on SDSS and UKIDSS data, [Bundy et al. \(2015\)](#) obtained stellar masses¹ and K-corrected colours after applying the SYNthetic aperture MAGnitudes software to match the photometry of two different facilities (SYN-MAGs, [Bundy et al. 2012](#)), and assuming a [Chabrier \(2003\)](#) initial mass function. The estimation of the stellar mass is more robust when using NIR data ([Courteau et al. 2014](#)): only objects that have at least one detection in one of the NIR bands of UKIDSS are considered for our analysis.

We derived the morphological parameters based on the CFHT/MegaPrime Stripe 82 (CS82) survey. CS82 has been designed to provide high quality *i*-band imaging for a large fraction of the Stripe 82 region, suitable for weak lensing measurements ([Kneib et al. in prep](#)). Due to the lensing specifications, an excellent image quality to a medium depth is required: the median seeing is $\sim 0''.6$ and the limiting magnitude $mag_{lim} \approx 24$ for point-like sources detection at 5σ . We run SExtractor² (v2.18.8, [Bertin & Arnouts 1996](#)) and PSFEX³ (v2.15.0, [Bertin 2011](#)) codes to characterize the morphology of all objects detected on the coadded images. Both codes have been designed to be run on large area images. SExtractor provides the morphological parameters by fitting defined brightness profiles, taking into account the point spread function (PSF) estimated by PSFEX. PSFEX and SExtractor were compared to the DAOPHOT and ALLSTAR software packages on simulated images by [Annunziatella et al. \(2013\)](#). They find that PSFEX performs accurate PSF modeling. Both codes were also used by [Desai et al. \(2012\)](#) to produce a PSF corrected model-fitting photometry catalogue of the Blanco Cosmology Survey.

The brightness profile of a galaxy is commonly fitted

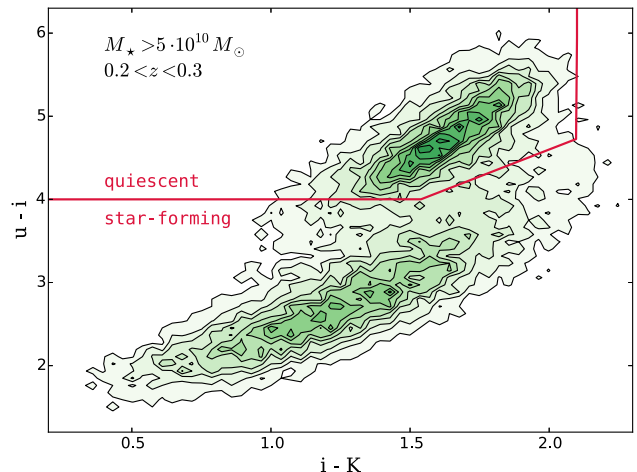


Figure 1. Colour-colour diagram that illustrates the bimodal behaviour of galaxies: star-forming late-type and quiescent early-type are located in two distinct locus. The red line shows the separation adopted to keep only quiescent objects. The green regions represent $\sim 60,000$ objects with redshift $0.2 < z < 0.3$, without mass cut. The colours have been K-corrected.

by the general Sérsic parametrization which depends on the Sérsic index n_{ser} . We fit four brightness profiles to the data: (1) a de Vaucouleurs ($n_{ser} = 4$) and (2) an exponential ($n_{ser} = 1$) profiles—which respectively suit the brightness profiles of early and late-type galaxies, (3) a general Sérsic profile and (4) a sum of a de Vaucouleurs and an exponential one. The morphological catalogue for the entire CS82 sample is based on the same approach as described in details in [Moraes et al. \(in prep\)](#). PSF extraction is the cornerstone of our search of compact elliptical galaxies. The PSFEX performances are assessed in [Moraes et al. \(in prep\)](#) by comparing the galaxy ellipticities recovered by PSFEX and SExtractor with the ellipticities obtained with *lens-fit* Bayesian shape measurement algorithm ([Heymans et al. 2012; Miller et al. 2013](#)) that we consider as a benchmark. We find a mean bias of the ellipticities of $\sim 0.01 \pm 0.05$ for PSF-size galaxies. Below the PSF, PSFEX and SExtractor still allow to recover the correct ellipticities, but within a larger error bar: $\sim 0.04 \pm 0.12$.

We measure the effective radius of the galaxies in the *i*-band. The pivot wavelength of *i*-band corresponds to rest-frame wavelengths of 635 nm and 477 nm at redshifts $z = 0.2$ and $z = 0.6$, respectively. According to [Kelvin et al. \(2012\)](#), the morphological K-correction resulting from this wavelength range is of the order of ~ 0.1 kpc for a spheroidal galaxy which effective radius is 1 kpc, and of the order of ~ 0.3 -kpc if the effective radius is 3 kpc. This 10 percent effect on the effective radius is of the order of the measurement error from SExtractor estimation.

2.2 Sample selection

The present analysis concentrates on the population of massive passive galaxies at intermediate redshift. It has been shown that the definition of the cuts applied has a large influence on the derived sample of compact massive quiescent galaxies, in particular the definition of the compactness and of the lower limit of the mass (e.g.,

¹ <http://massivegalaxies.com>

² <http://www.astromatic.net/software/sextractor>

³ <http://www.astromatic.net/software/psfex>

Damjanov et al. 2015). As we intend to compare our results with other studies (Quilis & Trujillo 2013; Carollo et al. 2013; van der Wel et al. 2014; van Dokkum et al. 2015), we have adopted different definitions described below. We applied therefore the following cuts on redshift (z), stellar mass (M_*) and colours:

(i) $0.2 < z < 0.6$. We are interested in the evolution of the population of massive galaxies between high and low redshifts. The limits have been set to fill the gap between these two regimes to follow Damjanov et al. (2013). Moreover our photometric redshift catalogue is trustworthy until $z \sim 0.6$.

(ii) $\log_{10}(M_*/M_\odot) > \log_{10}(M_{\min}/M_\odot)$. We note that to avoid contamination from star-forming galaxies, Moresco et al. (2013) recommend a cut of $\log_{10}(M_{\min}/M_\odot) = 10.75$ independently of the selection criteria to separate passive galaxies, and that is the reason why we have decided not to include a comparison with Barro et al. (2013) and Poggianti et al. (2013), who defined massive galaxies with a minimal mass of $\log_{10}(M_{\min}/M_\odot) = 10$ and 10.3, respectively. In the present analysis, we follow the definitions of Quilis & Trujillo (2013): $\log_{10}(M_{\min}/M_\odot) = 10.9$ (corresponding to $M_{\min} = 8 \times 10^{10} M_\odot$); Carollo et al. (2013): $\log_{10}(M_{\min}/M_\odot) = 10.5$; van der Wel et al. (2014): $\log_{10}(M_{\min}/M_\odot) = 10.7$ and van Dokkum et al. (2015): $\log_{10}(M_{\min}/M_\odot) = 10.6$.

(iii) The use of the colour bimodality to separate early-type quiescent galaxies to late-type star-forming ones has been first underlined by Strateva et al. (2001); Baldry et al. (2004). In more recent analyses, Wuyts et al. (2007); Williams et al. (2009); Whitaker et al. (2011); Muzzin et al. (2013) have worked in the rest frame colours $u - V$ vs. $V - J$. We follow their approach, applying adapted cuts for each bin of redshift, defining four slices of width equal to 0.1 between $z = 0.2$ and $z = 0.6$. To obtain the rest frame colours, a K-correction has been applied following the methodology of Chilingarian et al. (2010). As an example, we show in Figure 1 the cut applied for the bin of redshift $0.2 < z < 0.3$ in the colour-colour diagram $u - i$ vs. $i - K$, that has been defined to match roughly the minimum of the valley between the two clouds of points. For the redshifts ($0.3 < z < 0.6$), we chose $g - i$ for the y-axis. This ensures these colours encompass the rest-frame 4000 Å break, which strongly correlates with the age of the stellar population (e.g., Martin et al. 2007; Gonçalves et al. 2012). According to the availability of the NIR bands, we changed the x-axis for $i - H$ or $i - Y$.

2.3 Star/galaxy separation

Since we are searching for compact galaxies that may resemble point-like sources, it is of major importance to have an accurate star/galaxy discriminator. We base our star/galaxy discrimination on CS82 data for the first sorting. We refine it with colour information from SDSS/UKIDSS.

SEXTRACTOR in its model-fitting feature provides the SPREAD_MODEL parameter that estimates the similarity of the brightness profile of an object to the image PSF (see eq. 5 of Desai et al. 2012). Considering that CS82 images are built from four single exposures, dithered to fill the void between CCD chips and that our method is sensitive to PSF discontinuities that appear in these regions, we omit from our

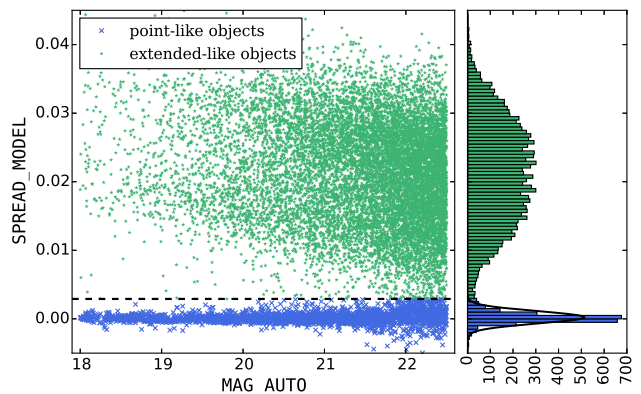


Figure 2. Distribution of the SPREAD_MODEL SEXTRACTOR parameter as a function of the Kron magnitude MAG_AUTO for one tile of the CS82 survey. A gaussian function has been fitted to the SPREAD_MODEL histogram of the stellar branch, and values greater than three sigma above that are defined as extended (green stars).

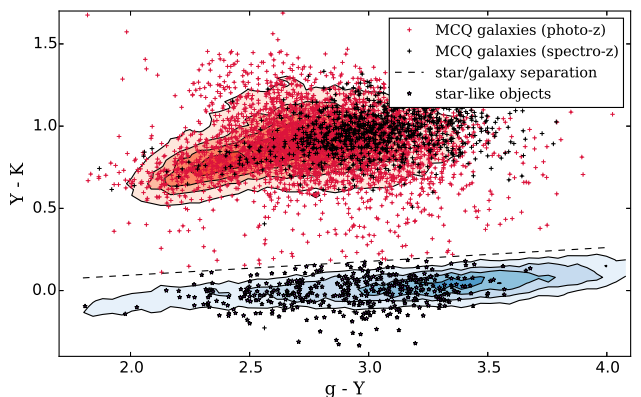


Figure 3. Colour-colour diagram $Y - K$ vs. $g - Y$ in which we refine our star/galaxy separation. Blue regions show the locus of high S/N stars ($S/N > 10$), whereas red regions indicate all massive quiescent galaxies ($M > 5 \times 10^{10} M_\odot$) with redshifts between 0.2 and 0.6.

search the ~ 33 percent of the total area corresponding to these interstitial regions.

The distribution of SPREAD_MODEL as a function of the SEXTRACTOR MAG_AUTO Kron magnitude is shown in Figure 2 for one coadded pointing (which we refer to as tile) of the CS82 survey that has been masked to get rid of bright saturated stars and PSF discontinuities. The stellar branch, for which SPREAD_MODEL ~ 0 , is clearly separated from values for extended objects until MAG_AUTO $\lesssim 22.5$.

For each tile we fit a gaussian function to the stellar branch, and consider as point-like objects those with a value of SPREAD_MODEL lower than three standard deviation from the mean of the gaussian. The median seeing of the CS82 survey is smaller than the median seeing of the SDSS⁴ (0.6 vs. ~ 1.43). Damjanov et al. (2013) showed that some compact galaxies are morphologically identified as stars by SDSS. We have checked that the only object of Damjanov et al. (2013) that lies in Stripe 82 has been well classified as an extended-

⁴ http://www.sdss.org/dr12/imaging/other_info/

like object using this procedure. However, its stellar mass being $\log_{10}(M_*) = 9.95$, it is not considered in our analysis.

A decontamination was required to eliminate misclassified stars as extended objects. We used the colour information provided by both SDSS and UKIDSS. Following Whitaker et al. (2011), the colours $u - J$ and $J - K$ are well adapted for a star/galaxy separation. Figure 3 shows the colour-colour diagram $g - Y$ and $Y - K$ of passive massive galaxies with redshifts $0.2 < z < 0.6$ (red regions). The stars selected with the morphological approach are shown in blue contours. Both datasets are clearly separated in this diagram. We define the separation between stars and galaxies by fitting a gaussian function of the projected histogram of the stellar cloud onto the y-axis, allowing for a 2σ variation. When Y or K bands were not available, we did the separation respectively in the following colours: $g - J/J - K$, $g - H/H - K$ and $g - Y/Y - H$. In the two last sets the separation between the stars and the galaxies is somehow less obvious. We checked that the colours of the galaxies that have spectroscopic data (and are identified as galaxies based on their spectral characteristics) lie in the correct region of the diagrams. We removed 2.6 percent of the objects of the quiescent catalogue (2,447 over 94,596) with this extra criterion.

2.4 Compactness criteria

As mentioned earlier, we follow the definitions of compactness adopted by Quilis & Trujillo (2013); Carollo et al. (2013); van der Wel et al. (2014) and van Dokkum et al. (2015). While Carollo et al. (2013) and van der Wel et al. (2014) opt for a criterion based on the non circularized effective radius R_{eff} , the others use the circularized effective radius $R_{\text{eff},c} = R_{\text{eff}} \times \sqrt{b/a}$ (b and a are respectively the minor and major axis of the model ellipse containing half of the total flux). A galaxy is considered as compact when:

- (i) Quilis & Trujillo (2013): $R_{\text{eff},c} < 1.5$ kpc;
- (ii) Carollo et al. (2013): we focus on the two lowest size bins of their Figure 4, for which the compact definitions correspond to $R_{\text{eff}} < 1.4$ kpc and $R_{\text{eff}} < 2.0$ kpc respectively, and to which we refer in Table 1 and Figure 12 as the ‘most’ and ‘less’ compact criteria respectively;
- (iii) van der Wel et al. (2014):

$$R_{\text{eff}} < A \times (M_*/10^{11} M_\odot)^{0.75}, \quad (1)$$

where R_{eff} is in kpc and $A = 1.5$ or 2.5 following respectively the most conservative (red dashed line in Figure 4) and the loosest (black short-dashed line) criteria of compactness;

- (iv) van Dokkum et al. (2015):

$$\log_{10}(R_{\text{eff},c}) < \log_{10}(M_*) - 10.7, \quad (2)$$

where $R_{\text{eff},c}$ is given in kpc and M_* in M_\odot .

We take the effective radius from the de Vaucouleurs fit of CS82 data using SEXTRACTOR and PSFEX for two reasons: this profile seems to be more robust than the general Sérsic one in the current version of SEXTRACTOR, and van der Wel et al. (2014) found that following the same colour selection to separate quiescent and star-forming galaxies as ours, they end up with a quiescent sample for which 80 percent of their Sérsic index is larger than 2.5. The

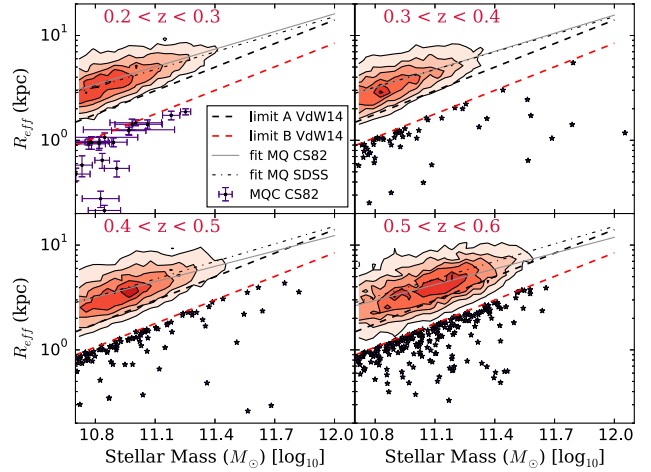


Figure 4. Galaxy size - mass relation in four redshift bins. Red regions show the quiescent galaxies, whereas the indigo stars are the compactest ones, according to the strictest criterion of van der Wel et al. (2014). The gray line is a fit of the red contours, the black short-dashed line shows the fit of Shen et al. (2003). Dashed red and black lines show the definition of the compactness by van der Wel et al. (2014). The error on the effective radius in kiloparsec (R_{eff}) depends on the error on the redshift and the measured effective radius in arcsecond (r_{eff}): $\delta R_{\text{eff}} (\text{kpc}) = (\delta r_{\text{eff}}/r_{\text{eff}} + \delta z/z) \times R_{\text{eff}}$. The error in stellar mass comes from the derivation of the mass with the SYNMAJ code.

galaxy size-mass distribution for massive quiescent galaxies is shown in Figure 4 for four bins of redshift between $0.2 < z < 0.6$. For readability, we only plot individually the most compact objects according to the van der Wel et al. (2014) criterion, and errors are shown only for the first bin of redshift. We verified that our size distribution reproduced the fit done by Shen et al. (2003) on SDSS data (gray line). We confirm the trend of decreasing sizes of early-type galaxies in the past (e.g., van der Wel et al. 2014; Furlong et al. 2015). The other compactness criteria are not shown here, however they behave similarly.

The percentage of compact galaxies among the total massive quiescent population is shown in Figure 5. Depending on the compactness definition, the sample of compact galaxies accounts for a few percent to 25 percent of all massive quiescent galaxies.

3 THE CATALOGUE OF COMPACT CANDIDATES

We give in Table 1 the number of massive quiescent galaxies and the number compact ones corresponding to each definition of compactness (Quilis & Trujillo 2013; Carollo et al. 2013; van Dokkum et al. 2015; van der Wel et al. 2014). The percentage of compact candidates which have SDSS spectra is shown. Within this section we only consider the catalogues obtained using the van der Wel et al. (2014) definitions for the compactness, as both criteria (the most and less conservative ones) are representative of the four chosen criteria of compactness. Using the CS82 morphological data, we end up with 424 massive quiescent candidate galaxies for the most compact criterion and 6596 candidates for the less compact one.

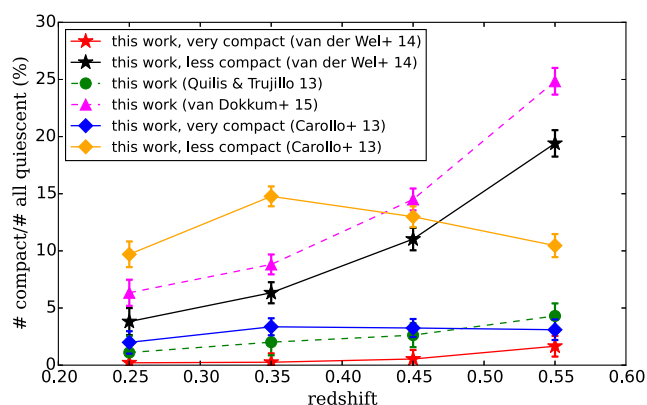


Figure 5. Redshift evolution between 0.2 and 0.6 of the ratio of the compact massive quiescent sample to the total number of massive quiescent galaxies. We show the ratio obtained for the different compactness criteria defined in the text and Poisson error bars.

Table 1. Number of massive quiescent galaxies above different minimum masses (M_{\min}) as defined by the different definitions adopted (C13: Carollo et al. 2013, vD15: van Dokkum et al. 2015, vdW14: van der Wel et al. 2014, QT13: Quilis & Trujillo 2013). ‘Most’ and ‘less’ refer to the most and less compact criteria (when it applies) as presented in section 2.4. The fourth column shows the number of massive compact quiescent candidates selected for each definition, and its respective percentage of galaxies having SDSS spectra.

M_{\min} $\log_{10}(M/M_{\odot})$	# quiescent	compact definition	# compact (with spectra)
10.5	78,493	C13 most	2,381 (0.3%)
		C13 less	9,766 (0.6%)
10.6	71,408	vD15	9,818 (23%)
10.7	62,515	vdW14 most	424 (8%)
		vdW14 less	6,596 (18%)
10.9	40,218	QT13	1,103 (2%)

3.1 Verifying the size estimates

Our selection of compact galaxies relies on size estimates extracted from ground-based images. As the effective radii are most of the time smaller than the full width half maximum (FWHM) of the PSF, we checked the reliability of the PSF deconvolution by the PSFEX package by comparing the results with space based images of higher quality. We collected HST images taken with the Advanced Camera for Surveys (ACS) Wide field Channel (WFC) in the i -bands (nominally the F814W and F775W filters) from the Hubble Legacy Archive.⁵ Thirteen of our massive compact candidates within the less conservative sample have been covered by HST. The images come from different observing programs and their exposure time varies between 1,000 and 7,866 seconds, corresponding respectively to depths of ~ 23.5 and 24.5 in i -band for extended sources. We estimated the morphological parameters by running SEXTRACTOR and PSFEX on each HST image. All compact candidates are indeed extended objects (i.e., not stars), as shown in Figure 6. The

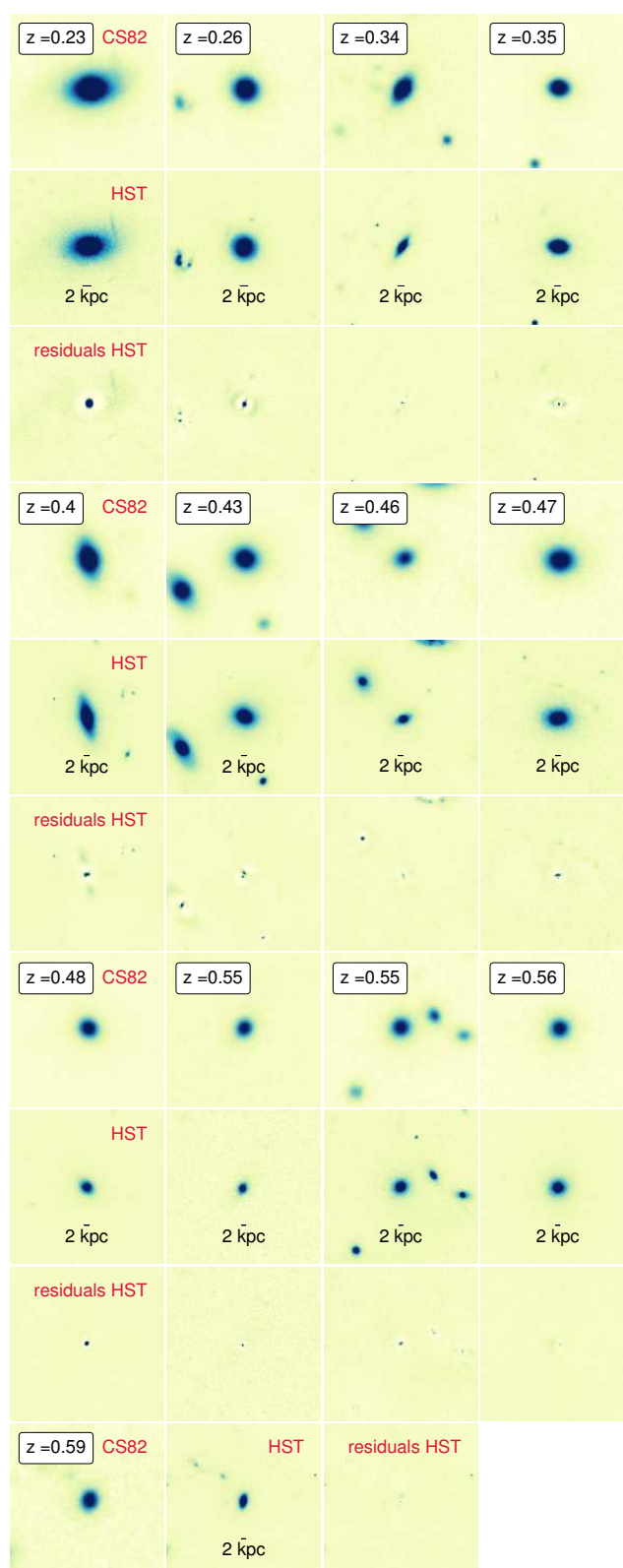


Figure 6. Compact massive quiescent galaxies that have been observed by both CS82 (first, fourth, seventh and tenth lines) and HST/ACS (second, fifth, eighth and tenth lines) in i -band. The images are centred on the galaxy of interest. The residuals of the fitting of the HST images by a de Vaucouleurs brightness profile are shown (third, sixth, ninth and tenth lines). The cutouts are north-oriented, with a side size of $10''$. An inset bar indicates the size of 2 kpc at the redshift of the galaxies.

⁵ <http://hla.stsci.edu>

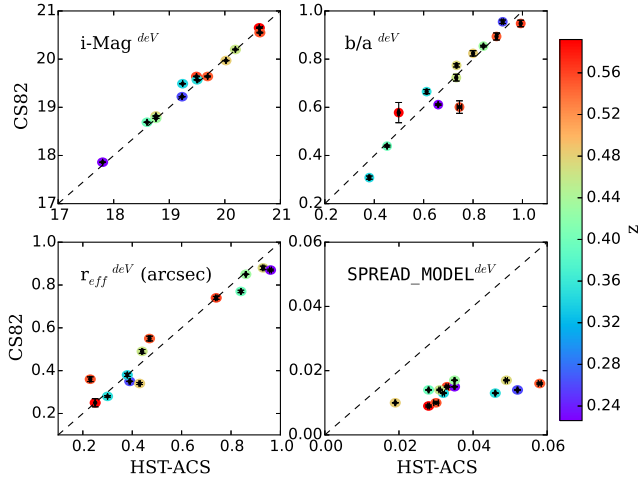


Figure 7. Comparison of the morphological and photometric properties of the compact galaxies that have been observed both by CS82 and HST. The parameters were derived by fitting a de Vaucouleurs brightness profile using SEXTRACTOR and PSFEX: model magnitude (upper left), aspect ratio b/a (upper right), effective radius r_{eff} (lower left) and the `SPREAD_MODEL` parameter (lower right). The colour scale indicates the redshift.

redshifts indicated in boxes are spectroscopic (SDSS/BOSS) for four of them (the ones with $z = 0.4, 0.47, 0.56$ and the second in the row with $z = 0.55$), and photometric for the remaining nine.

We compare the morphological outputs from SEXTRACTOR obtained by fitting a de Vaucouleurs profile on both sets of images (see Figure 7). The photometry and the morphology extracted from both CS82 and HST/ACS data are in very good agreement. We report a mean squared difference of 0.10 in magnitude and of 0.4 kpc for the effective radius. We do not identify clear systematics due to the larger PSF of CS82 images and we verify the robustness of the PSF deconvolution by the PSFEX code. The `SPREAD_MODEL` parameters derived from the HST images are larger than the CS82 as the galaxies are clearly resolved as extended sources.

We also compare the morphological parameters derived by SEXTRACTOR and PSFEX with those from the SDSS. We have therefore confronted our effective radii to the one coming from SDSS DR12 database (`deVRad_i` from CasJobs, description in Stoughton et al. 2002). All effective radii are not circularized and come from a de Vaucouleurs fit deconvolving the PSF. We find a good correlation and a small systematic offset of $\sim 0''.03$ between the effective radii of all quiescent massive ($\log_{10}(M_*/M_\odot) > 10.6$) galaxies of both datasets. This offset might be related to the offset observed in magnitude (see Moraes et al. in prep) which is expected to be produced by the truncation beyond $7R_{\text{eff}}$ by SDSS. Figure 8 shows the result of this comparison. As the median seeing of SDSS is $1''.43$ (Stoughton et al. 2002), we cannot rely on the SDSS morphology for small effective radii. Nevertheless, we still can confirm that for larger radii the correlation is correct. The compact sample following the loosest van der Wel et al. (2014) criterion is shown with black crosses: their effective radii are well below the SDSS median seeing.

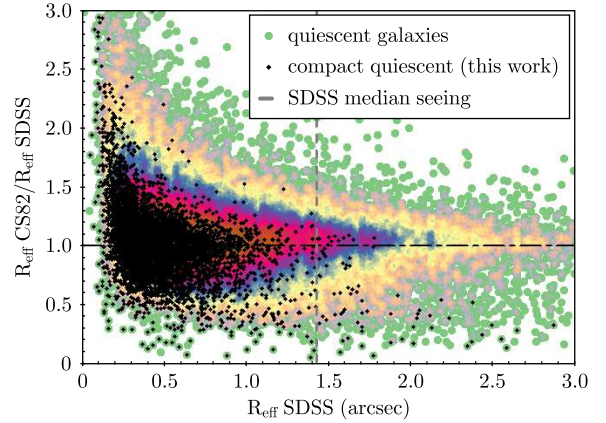


Figure 8. Comparison of the effective radii of massive quiescent galaxies obtained from a de Vaucouleurs fit, from SDSS and CS82 data. The ratio of the effective radii is shown as a function of the effective radius in SDSS, the colour gradient scales with the galaxy number. The median seeing of SDSS is represented by a grey dashed line. Compact massive quiescent galaxies defined by the van der Wel et al. (2014) loosest criterion are shown as black points.

3.2 Morphological properties

Two of the authors (AC and EG) visually inspected each of the most and less compact candidates, examining the object and its morphological model. They agree on the following classification within an error of ~ 3 percent and find that:

- (i) ~ 82 percent have a typical elliptical shape and good residuals;
- (ii) ~ 11 percent have bad residuals due to close neighbours. SEXTRACTOR is currently not able to handle a simultaneous fit of various objects: pixels of the segmentation maps are attributed to only one object, even if receiving signal from two sources;
- (iii) ~ 7 percent have bad residuals due to the non adequacy of the de Vaucouleurs shape to fit the galaxy brightness profile.

We checked that the colours of these three categories were equally distributed in the colour-colour diagram used for the star-forming/quiescent separation. In addition to the de Vaucouleurs brightness profile, we fit a general Sérsic profile to all the objects using SEXTRACTOR. We present in Figure 9 the Sérsic index distribution as a function of the aspect ratio (axial ratio of the best-fitting model) for the sample of most and less compact galaxies in red contours and blue colours, respectively (most compact galaxies are included in the less compact sample). Our most and less compact massive quiescent candidates have a high median Sérsic index ($\langle n_{\text{ser}} \rangle = 6.9$ and $\langle n_{\text{ser}} \rangle = 5.2$ respectively) characteristic of early-type galaxies ($n_{\text{ser}} \geq 2.5$); they also present a roundish shape, with a median aspect ratio of $\langle b/a \rangle = 0.66$ and $\langle b/a \rangle = 0.71$ respectively.

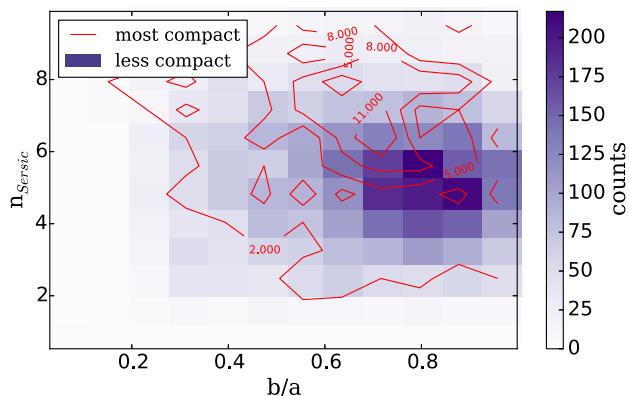


Figure 9. Distribution of the Sérsic index as a function of the aspect ratio of the selected compact passive galaxies, extracted from a fit by a general Sérsic brightness profile. The blue 2D-histogram shows the less compact sample, whereas the red contours represent the most compact candidates. We notice that most compact galaxies are included in the less compact sample.



Figure 10. Combined masks from CS82 and UKIDSS in a portion of Stripe 82 for the estimation of the effective area.

4 NUMBER DENSITY EVOLUTION

4.1 Effective area

One characteristic that sets this study aside from other works (e.g., Valentinuzzi et al. 2010a,b; Poggianti et al. 2013; Damjanov et al. 2014; Tortora et al. 2016) is the uniform coverage of a large contiguous region of the sky, without pre-selection based on the environment. To calculate the evolution of the density of compact galaxies with redshift, we first estimate the area covered by the CS82 survey. We combined the masks of UKIDSS and CS82 using the WEIGHTWATCHER⁶ and SWARP⁷ packages. WEIGHTWATCHER is designed to combine weight maps, flag maps and polygons, whereas SWARP re-samples and coadds FITS images. These masks were produced to remove bright stars, cosmic rays and artefacts. We also removed the regions between CCD chips from CS82, where the PSF is not correctly reconstructed. We show a portion of the total mask in Figure 10: the horizontal and vertical lines correspond to the inter-CCD regions. We have measured an effective area of $A_{\text{eff}} = 82.6 \pm 7.3 \text{ deg}^2$.

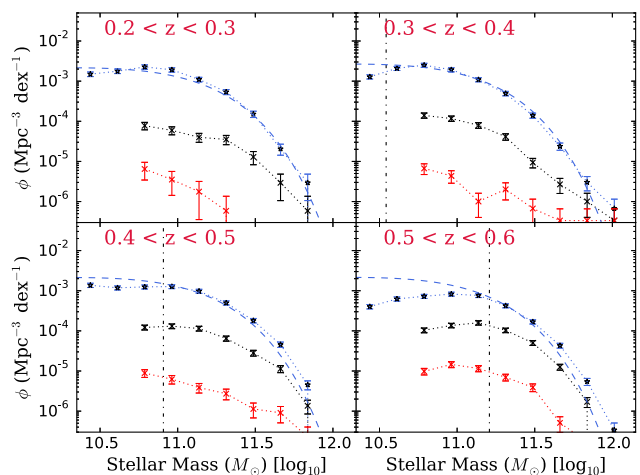


Figure 11. Galaxy stellar mass functions (GSMF) in four bins of redshift between $z = 0.2$ and $z = 0.6$. Blue upper point represent the quiescent selections, lower red and middle black points show respectively the most and less compact massive candidates obtained adopting the van der Wel et al. (2014) criteria. Vertical magenta dash-dotted lines show the limiting mass above which the quiescent sample is complete. Blue dashed lines are double Schechter functions fitted to quiescent GSMF data, whose parameters are taken from Ilbert et al. (2013).

4.2 Completeness

Our sample of compact massive quiescent galaxies suffers incompleteness at the low mass end due to the magnitude limit of the NIR data (optical data are deeper). We derive a 80 percent completeness limit in i -band of ~ 20.5 for extended sources by looking at the inflection in the number counts. This magnitude limit in i -band corresponds to an increasing limiting stellar mass at increasing redshifts, above which we consider that the sample of quiescent galaxies is complete. The limiting stellar mass is defined as in Pozzetti et al. (2010): for each bin of redshift in $z = [0.2, 0.3, 0.4, 0.5, 0.6]$ we compute the upper envelope of the limiting mass distribution for 95 percent completeness and find respectively 10.2, 10.5, 10.9 and 11.2 (in $\log_{10} M_*/M_\odot$). These values are represented by vertical lines in Figure 11 and summarized in Table 2.

We compute the galaxy stellar mass function (GSMF) following the V_{max} method (Schmidt 1968; Baldry et al. 2008):

$$\Phi_{\log_{10} M} = \frac{1}{\Delta \log_{10} M} \sum_i \frac{1}{V_{\text{max},i}}, \quad (3)$$

where $\Delta \log_{10} M$ is the mass bin in logarithmic scale. $V_{\text{max},i}$ is the comoving volume over which the i th galaxy could be observed and is computed given the redshift of the galaxy and the limiting magnitude of the survey (21.0 in mag i at 50 percent completeness). Our quiescent GSMF is shown in Figure 11 as blue stars in different redshift bins. To estimate how much of the passive galaxy population we are losing at higher redshift towards the lower masses, we assume that the shape of the GSMF does not vary significantly between

⁶ <http://www.astromatic.net/software/weightwatcher>

⁷ <http://www.astromatic.net/software/swarp>

Table 2. Limiting stellar mass, for each redshift bin, above which the sample of quiescent galaxies is complete, and factor of completeness for subsets of galaxies above a given minimum stellar mass ($10^{10.5}$, $10^{10.6}$, $10^{10.7}$ and $10^{10.9} M_{\odot}$).

z bin	limiting mass $\log_{10}(M_{*}/M_{\odot})$	completeness factor for $\log_{10}(M_{*}/M_{\odot})$			
		> 10.5	> 10.6	> 10.7	> 10.9
0.2-0.3	10.18	1	1	0.99	0.97
0.3-0.4	10.54	1	0.99	0.97	0.96
0.4-0.5	10.91	0.73	0.84	0.95	1
0.5-0.6	11.21	0.57	0.59	0.63	0.80

$z = 0.2$ and $z = 0.6$, and that we can simply renormalise the double Schechter function provided by [Ilbert et al. \(2013\)](#). This renormalization is shown as blue dashed lines in Figure 11, where we have only included in the fit the data points that are above the limiting mass. We define the completeness factor as the ratio of the number of detected galaxies over the number of expected galaxies according to the Schechter function. Completeness factors computed for different minimum stellar masses ($10^{10.5}$, $10^{10.6}$, $10^{10.7}$ and $10^{10.9} M_{\odot}$) are summarized in Table 2. We find that we are complete towards lower redshifts where completeness factors are close or equal to one for all the chosen minimum stellar masses of our samples. We miss less massive galaxies in number count at higher redshifts: for the bin $0.5 < z < 0.6$ our selection of quiescent galaxies is complete at 57% above $10^{10.5} M_{\odot}$ and at 80% above $10^{10.9} M_{\odot}$.

We take into account these completeness factors in the estimation of the number densities that are shown on Figures 12 and 13 where the raw number count of compact quiescent galaxies above a given stellar mass in a given redshift bin is divided by the appropriate completeness factor taken from Table 2. We have calculated the influence of the slope of the GSMF at the low mass end on the number density of compact massive galaxies by artificially changing the limiting stellar mass within the stellar mass median error ($d\log_{10}(M_{*}/M_{\odot}) = 0.09$). The value of the resulting error on the number density depends on the chosen compactness definition and on the redshift bin, of the order of ~ 10 percent. This error is included in the Figures 12 and 13.

For illustration purposes, we also compute the compact quiescent GSMF for the samples following the [van der Wel et al. \(2014\)](#) compactness definition. Less (black crosses) and most (red crosses) compact candidates are shown in Figure 11. They follow the global behaviour of quiescent galaxies. In the lower redshift bin ($0.2 < z < 0.3$) the knee of the GSMF is only visible for the less compact sample.

4.3 Results

In Figure 12 we compare our results for the variation of the number density of massive quiescent compact galaxies in the Stripe 82 over the redshift range $0.2 < z < 0.6$ to their counterparts at higher redshifts in the literature, using the same definitions of compactness ([Carollo et al. 2013](#); [van der Wel et al. 2014](#); [van Dokkum et al. 2015](#)). We observe that the density of massive compact quiescent galaxies at intermediate redshifts decreases towards lower redshifts

for two of the compactness criteria ([van der Wel et al. 2014](#); [van Dokkum et al. 2015](#)), while it remains approximately constant following the criteria of [Carollo et al. \(2013\)](#). We find that the number density of the most compact samples of [van der Wel et al. \(2014\)](#) and [Carollo et al. \(2013\)](#) are respectively 1.3 dex and 0.8 smaller than the number density of their corresponding less compact selections. Both the minimal mass of the sample and the compactness definition have an influence on the behaviour of the derived number density of compact massive galaxies. Within the error bars, we confirm the trend observed by [Carollo et al. \(2013\)](#) from redshifts $z = 1.0$: the number density of compact galaxies with a mass larger than $10^{10} M_{\odot}$ is roughly stable since redshift $z \sim 0.8$. Our data do not connect easily to other higher redshift data: [van der Wel et al. \(2014\)](#) and [van Dokkum et al. \(2015\)](#) observe the beginning of a decrease at redshift $z \sim 1.5$ that leads to values at intermediate redshifts that are lower by a factor $\sim 5 - 6$ than our observations. However, [Damjanov et al. \(2015\)](#) observe the same trend as us at intermediate redshifts working on the COSMOS field and applying the compactness criteria of [van der Wel et al. \(2014\)](#), albeit with larger error bars. The gap is likely due to the limited volume of CANDELS at intermediate redshifts or to a bias in the sample selection and definition. We observe the same trend as [Cassata et al. \(2013\)](#): the number density of smaller early-type galaxies evolves more rapidly than that of larger ones. We do not compare directly our density with their result as they adopt a minimal stellar mass of $10^{10} M_{\odot}$, that we consider to be too low in the context of our paper.

Current N-body simulations have provided some clues to understand the evolution of the population of compact massive quiescent galaxies with cosmic times. [Furlong et al. \(2015\)](#) have applied the less conservative criterion of compactness of [van der Wel et al. \(2014\)](#). The gravitational force softening length (i.e. the spatial resolution) of the largest EAGLE simulation used in their analysis is $\epsilon = 0.70$ kpc. They test the convergence of their results by comparing runs of various resolutions. Below the resolution of the simulations, subgrid models are applied. The gravitational softening is smaller than the strongest criteria of [van der Wel et al. \(2014\)](#), making them adequate for comparison. They find that the number density of compact massive quiescent galaxies increases for decreasing redshifts until $z \sim 0.7$, then declines for $z < 0.8$. At high redshifts, the discrepancy between their data and the observed density by [van der Wel et al. \(2014\)](#) is likely due to the limited box size of the simulation. However, we emphasize that the comparison with observations is not that simple, because the determination of the effective radius and the stellar mass are done in different ways. We show the comparison of our measurements at intermediate redshifts with EAGLE measurements in Figure 13. At intermediate redshifts, they expect a continuous decrease of the number density of massive compact galaxies that we do observe in our study but with an offset of ~ 0.7 dex. [Quilis & Trujillo \(2013\)](#) used semianalytical models based on the Millenium simulation to calculate the expected fraction of massive compact galaxies that remain almost untouched since redshifts $z > 2$, i.e. that evolve in stellar mass by less than 30 percent. Applying similar cuts in mass and circularized effective radii (see sections 2.2 and 2.4), we obtain number densities that are within the er-

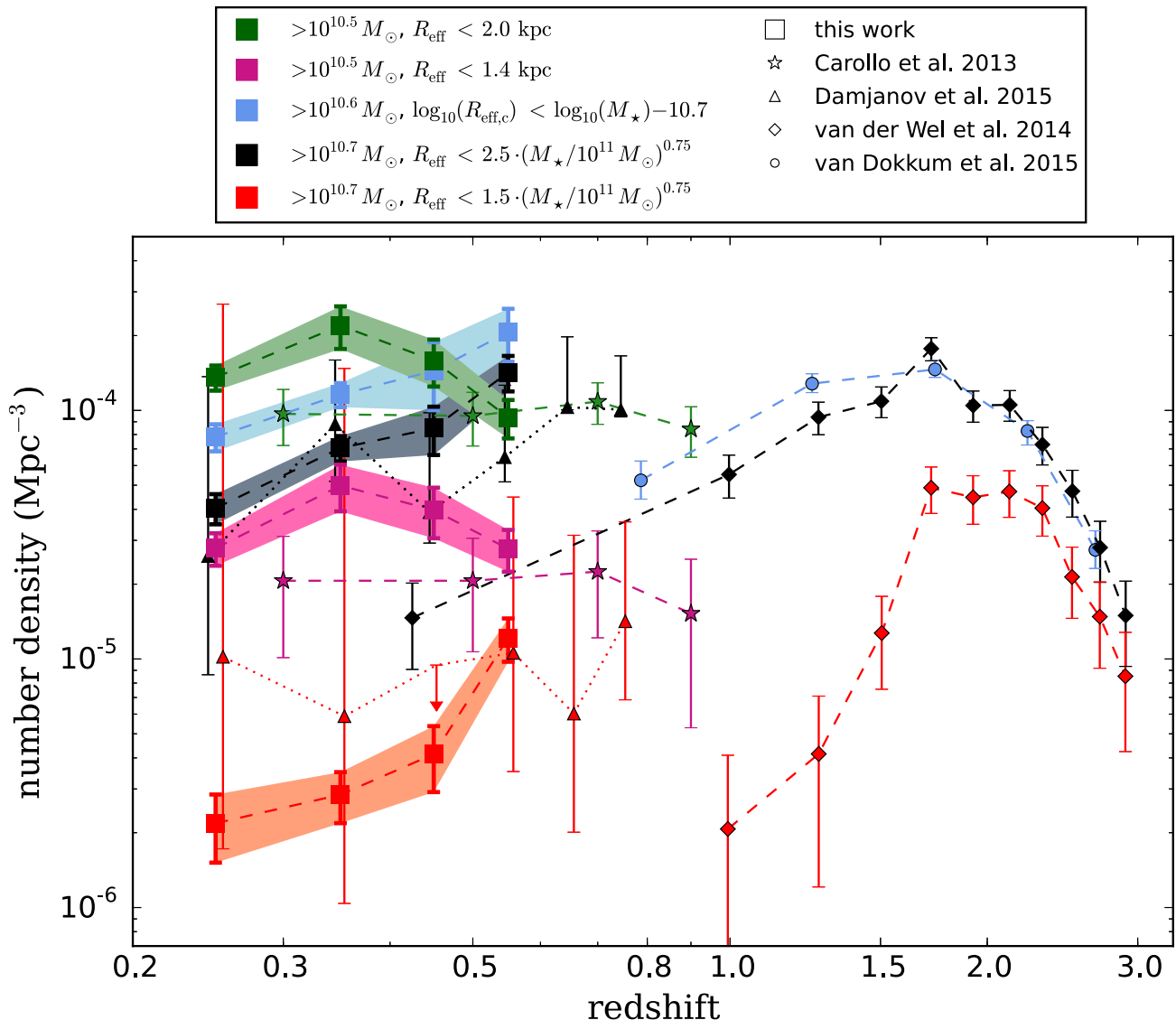


Figure 12. Evolution of the number density of quiescent compact massive galaxies down to redshift 3. Different colours indicate different definitions of compactness: red and black for the most and less conservative criteria of [van der Wel et al. \(2014\)](#) respectively (see section 2.4), blue refers to the one adopted by [van Dokkum et al. \(2015\)](#), pink and green to the most and less conservative criteria of [Carollo et al. \(2013\)](#) respectively. Density obtained with CS82 data are shown with large squares (this work), diamonds represent [van der Wel et al. \(2014\)](#) data, circles [van Dokkum et al. \(2015\)](#) and stars [Carollo et al. \(2013\)](#) ones. At intermediate redshifts we also plot as triangles the results of [Damjanov et al. \(2015\)](#) based on the COSMOS data, following the same colour code.

ror bars of the expected value of [Quilis & Trujillo \(2013\)](#) and that follow the same trend. Finally [Wellons et al. \(2016\)](#) also predict that the number density of compact massive quiescent galaxies should decrease in the local universe; although they attribute this to the processes that galaxies undergo during their evolution, they provide no further quantification of these conclusions.

We investigate the parameter of the compact massive galaxy definition that lead to different behaviours of the number density at intermediate redshifts. We identify that the increase of the number density is strongly related to the lower limit in mass of the sample of massive galaxies. Applying the minimal masses of [van der Wel et al. \(2014\)](#)

and [Quilis & Trujillo \(2013\)](#) as defined in Section 2.2 associated to the compact criterion of [Carollo et al. \(2013\)](#), we do observe an increase of the number density of compact massive quiescent galaxies at intermediate redshifts. This is confirmed by [Carollo et al. \(2013\)](#) concerning their most massive sample of compact quiescent galaxies.

5 DISCUSSION AND CONCLUDING REMARKS

Hydrodynamical simulations suggest that the compact passive massive galaxy population is continuously evolving. According to [Furlong et al. \(2015\)](#) and [Wellons et al. \(2016\)](#)

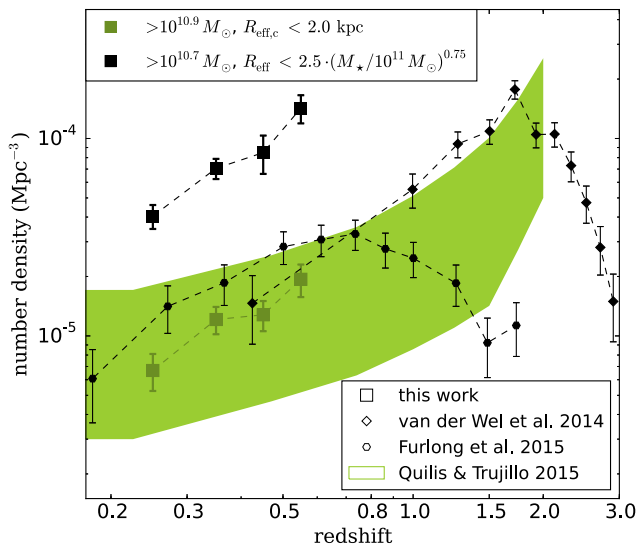


Figure 13. Evolution over cosmic times of the number density of compact massive quiescent galaxies. Our results are compared with simulations. Large squares present this work, following two different compactness definitions: in black the loosest definition of [van der Wel et al. \(2014\)](#) and in green the one of ([Quilis & Trujillo 2013](#)). The green area shows the expectations of [Quilis & Trujillo \(2013\)](#). Black hexagons show the prediction of [Furlong et al. \(2015\)](#) in the context of the EAGLE hydrodynamical simulation. Black diamonds show the less compact criterion of [van der Wel et al. \(2014\)](#).

the main size growth mechanisms of passive galaxies between $z > 1.5$ and $z = 0$ are acquisition of ex-situ stars through dry-mergers events and renewed star formation events also triggered by mergers. Thus very few will have been left untouched with cosmic time, making untouched relics very rare. Studying the number density evolution of compact massive relics is unlikely to reflect the evolution of individual galaxies, but instead gives indications about the frequency of the merging processes that this population encounters over cosmic times. Comparing our results with simulations, we thus confirm the stochastic behaviour of the minor merging processes. We indeed observe a constant decrease of the number density of this galaxy population at intermediate redshifts, and notice that the normalization and the behaviour of the number density is clearly sensitive to the definitions adopted to characterize compact relics. We therefore agree with the conclusions of [Carollo et al. \(2013\)](#): we indeed find that newly quenched galaxies may have typical sizes larger than high redshift ones to explain the progressive disappearance of compact massive galaxies. We however observe an individual evolution of this relic population, that is confirmed by adopting minimal masses larger than $M_* > 5 \times 10^{10} M_\odot$ instead of $M_* > 3 \times 10^{10} M_\odot$ as in [Carollo et al. \(2013\)](#). The number density of compact quiescent galaxies is particularly sensitive to the interval of mass considered.

The population of compact galaxies at intermediate redshifts is scarce and therefore requires a large survey area to have enough statistics. Stripe 82 data complies with many crucial points in this context and allow us to reduce significantly the error bars on the compact relics num-

ber density. We note an offset between our observations and [Furlong et al. \(2015\)](#) predictions (see Figure 13) and attribute it to potential environmental effects, considering that the volume probed by hydrodynamical simulations is smaller than ours. This effect known as cosmic variance has a influence on galaxy population properties. [Moster et al. \(2011\)](#) show that for the COSMOS, EGS and GOODS fields, we should expect an cosmic variance of respectively ~ 0.2 , ~ 0.25 and ~ 0.35 for massive galaxies at intermediate redshifts. Moreover, as underlined by [Stringer et al. \(2015\)](#), [Wellons et al. \(2016\)](#) and [Peralta de Arriba et al. \(2016\)](#), the environment of compact galaxies plays a critical role with respect to their potential survival. We note that although these studies all agree on this matter, they have conflicting conclusions on the specifics: the first study alleges that isolated galaxies are more likely to be protected from merger events, whereas the other two studies point to the dense central regions of galaxy clusters as the most likely places to find relics. In a future paper we envisage exploring the impact of environment on the compact galaxy population in the context of the Stripe 82 survey.

Despite the fact that we have based our analysis on ground based images of excellent quality, we cannot exclude that there is possible contamination in our sample coming from stars and from inaccurate morphological parameters. Size estimation might be a source of systematics, in particular for galaxies that have close neighbours; these represent ~ 11 percent of the total sample.

In this paper, we have identified a population of quiescent massive compact galaxies at intermediate redshifts, making use of the exceptional multiwavelength coverage of the equatorial region called Stripe 82. Morphological parameters were derived running SEXTRACTOR and PSFEX codes on CFHT/Megacam deep i -band images from CS82. We apply different definitions of compactness to compare our results to previous studies. We find that:

(i) We observe a strong dependence of the absolute number density of compact massive galaxies with the adopted compactness definition. It varies e.g. by a factor of ~ 80 between the [Carollo et al. \(2013\)](#) and the strictest [van der Wel et al. \(2014\)](#) definitions. This variation is significantly larger than the errors on the number density.

(ii) The number density of compact massive galaxies evolves relatively slowly at intermediate redshifts. It decreases with cosmic time by a factor of ~ 5 between $z = 0.6$ and $z = 0.2$ when adopting the [van der Wel et al. \(2014\)](#) or [van Dokkum et al. \(2015\)](#) definitions, and remains constant within error bars according to the compactness definition of [Carollo et al. \(2013\)](#). We note that the evolution of the number density with redshifts is significantly smaller than the absolute variation due to the adopted compactness definition.

(iii) A significant offset in number density is observed between our measurements at intermediate redshifts and previous works. We systematically find larger number density by a factor of ~ 5 compared to [van der Wel et al. 2014](#) and [van Dokkum et al. 2015](#) at $z \sim 0.6$. Cosmic variance might explain this difference as our volume at that redshift is ~ 330 times larger than the CANDELS one. Our measurements at $z = 0.6$ are therefore roughly compatible with the number

densities obtained at redshifts 1.5-2 by [van der Wel et al. 2014](#) and by [van Dokkum et al. 2015](#). This lack of evolution suggests that most of the size evolution observed in these populations is due to progenitor bias. Only the abundance of extreme compact galaxies (the most compact galaxies of [van der Wel et al. 2014](#)) seem to have dropped by a factor of 20 since $z = 2$. This is likely due to the disappearance of very compact progenitors below $z < 2$ and to the global size growth of early type galaxies over cosmic times. This confirms the stochastic behaviour of merging processes observed by hydrodynamical and cosmological simulations.

ACKNOWLEDGEMENTS

We thank our anonymous referee for useful comments that improved this paper. AC is supported by the Brazilian Science Without Borders program, managed by the Coordenação de Aperfeiçoamento de Pessoal de Nível Superior (CAPES) foundation, and the Conselho Nacional de Desenvolvimento Científico e Tecnológico (CNPq) agency. Fora Temer. MM is partially supported by CNPq (grant 312353/2015-4) and FAPERJ (grant E-26/110.516/2-2012). TE is supported by the Deutsche Forschungsgemeinschaft in the framework of the TR33 ‘The Dark Universe’. HHi acknowledges support from the DFG under Emmy Noether grant Hi 1495/2-1. HYS acknowledges the support from Marie-Curie International Incoming Fellowship (FP7-PEOPLE-2012-IIIF/327561) and NSFC of China under grants 11103011. CBG acknowledges financial support from PRIN-INAF 2014 1.05.01.94.02. We thank I. Trujillo and the LASEX⁸ members for fruitful discussions. This work is based on observations obtained with MegaPrime/MegaCam, a joint project of CFHT and CEA/DAPNIA, at the Canada-France-Hawaii Telescope (CFHT), which is operated by the National Research Council (NRC) of Canada, the Institut National des Sciences de l’Univers of the Centre National de la Recherche Scientifique (CNRS) of France, and the University of Hawaii. The Brazilian partnership on CFHT is managed by the Laboratório Nacional de Astrofísica (LNA). We thank the support of the Laboratório Interinstitucional de e-Astronomia (LIneA). We thank the CFHTLenS team.

REFERENCES

- Abazajian K. N., et al., 2009, *ApJS*, **182**, 543
 Annis J., et al., 2014, *ApJ*, **794**, 120
 Annunziatella M., Mercurio A., Brescia M., Cavuoti S., Longo G., 2013, *PASP*, **125**, 68
 Baldry I. K., Glazebrook K., Brinkmann J., Ivezić Ž., Lupton R. H., Nichol R. C., Szalay A. S., 2004, *ApJ*, **600**, 681
 Baldry I. K., Glazebrook K., Driver S. P., 2008, *MNRAS*, **388**, 945
 Barro G., et al., 2013, *ApJ*, **765**, 104
 Bertin E., 2011, in Evans I. N., Accomazzi A., Mink D. J., Rots A. H., eds, *Astronomical Society of the Pacific Conference Series Vol. 442, Astronomical Data Analysis Software and Systems XX*. p. 435
 Bertin E., Arnouts S., 1996, *A&AS*, **117**, 393
 Brammer G. B., van Dokkum P. G., Coppi P., 2008, *ApJ*, **686**, 1503
 Bruce V. A., et al., 2012, *MNRAS*, **427**, 1666
 Bundy K., Hogg D. W., Higgs T. D., Nichol R. C., Yasuda N., Masters K. L., Lang D., Wake D. A., 2012, *AJ*, **144**, 188
 Bundy K., et al., 2015, *ApJS*, **221**, 15
 Carollo C. M., et al., 2013, *ApJ*, **773**, 112
 Cassata P., et al., 2013, *ApJ*, **775**, 106
 Chabrier G., 2003, *PASP*, **115**, 763
 Chilingarian I. V., Melchior A.-L., Zolotukhin I. Y., 2010, *MNRAS*, **405**, 1409
 Cimatti A., et al., 2004, *Nature*, **430**, 184
 Cimatti A., et al., 2008, *A&A*, **482**, 21
 Citro A., Pozzetti L., Moresco M., Cimatti A., 2016, preprint, ([arXiv:1604.07826](#))
 Collister A. A., Lahav O., 2004, *PASP*, **116**, 345
 Courteau S., et al., 2014, *Reviews of Modern Physics*, **86**, 47
 Daddi E., et al., 2005, *ApJ*, **626**, 680
 Damjanov I., et al., 2009, *ApJ*, **695**, 101
 Damjanov I., et al., 2011, *ApJ*, **739**, L44
 Damjanov I., Chilingarian I., Hwang H. S., Geller M. J., 2013, *ApJ*, **775**, L48
 Damjanov I., Hwang H. S., Geller M. J., Chilingarian I., 2014, *ApJ*, **793**, 39
 Damjanov I., Geller M. J., Zahid H. J., Hwang H. S., 2015, *ApJ*, **806**, 158
 Dark Energy Survey Collaboration et al., 2016, *MNRAS*, **460**, 1270
 Dawson K. S., et al., 2013, *AJ*, **145**, 10
 Dekel A., Burkert A., 2014, *MNRAS*, **438**, 1870
 Desai S., et al., 2012, *ApJ*, **757**, 83
 Diemand J., Moore B., 2011, *Advanced Science Letters*, **4**, 297
 Drinkwater M. J., et al., 2010, *MNRAS*, **401**, 1429
 Eisenstein D. J., et al., 2011, *AJ*, **142**, 72
 Fliri J., Trujillo I., 2016, *MNRAS*, **456**, 1359
 Förster Schreiber N. M., et al., 2014, *ApJ*, **787**, 38
 Franx M., van Dokkum P. G., Förster Schreiber N. M., Wuyts S., Labbé I., Toft S., 2008, *ApJ*, **688**, 770
 Furlong M., et al., 2015, preprint, ([arXiv:1510.05645](#))
 Garilli B., et al., 2008, *A&A*, **486**, 683
 Gonçalves T. S., Martin D. C., Menéndez-Delmestre K., Wyder T. K., Koekemoer A., 2012, *ApJ*, **759**, 67
 Graham A. W., Dullo B. T., Savorgnan G. A. D., 2015, *ApJ*, **804**, 32
 Heymans C., et al., 2012, *MNRAS*, **427**, 146
 Heywood I., et al., 2016, *MNRAS*, **460**, 4433
 Huertas-Company M., et al., 2013, *MNRAS*, **428**, 1715
 Huertas-Company M., et al., 2015, *ApJ*, **809**, 95
 Ilbert O., et al., 2013, *A&A*, **556**, A55
 Jiang L., et al., 2014, *ApJS*, **213**, 12
 Kelvin L. S., et al., 2012, *MNRAS*, **421**, 1007
 LSST Science Collaboration et al., 2009, preprint, ([arXiv:0912.0201](#))
 LaMassa S. M., et al., 2013, *MNRAS*, **436**, 3581
 Lawrence A., et al., 2007, *MNRAS*, **379**, 1599
 Lilly S. J., Carollo C. M., 2016, preprint, ([arXiv:1604.06459](#))
 Longhetti M., et al., 2007, *MNRAS*, **374**, 614
 Madau P., Dickinson M., 2014, *ARA&A*, **52**, 415
 Madau P., Pozzetti L., Dickinson M., 1998, *ApJ*, **498**, 106
 Martin D. C., et al., 2007, *ApJS*, **173**, 342
 Miller L., et al., 2013, *MNRAS*, **429**, 2858
 Mo H. J., Mao S., White S. D. M., 1998, *MNRAS*, **295**, 319
 Moresco M., et al., 2013, *A&A*, **558**, A61
 Moster B. P., Somerville R. S., Newman J. A., Rix H.-W., 2011, *ApJ*, **731**, 113
 Muzzin A., et al., 2013, *ApJS*, **206**, 8
 Newman A. B., Ellis R. S., Treu T., Bundy K., 2010, *ApJ*, **717**, L103

⁸ <http://dgp.cnpq.br/dgp/espelhogrupo/5167044310442074>, Laboratório de Astrofísica Extragaláctica do Observatório do Valongo

- Oser L., Naab T., Ostriker J. P., Johansson P. H., 2012, *ApJ*, **744**, 63
- Papovich C., et al., 2016, *ApJS*, **224**, 28
- Peng Y.-j., et al., 2010, *ApJ*, **721**, 193
- Peralta de Arriba L., Quilis V., Trujillo I., Cebrián M., Balcells M., 2016, preprint, ([arXiv:1605.06503](https://arxiv.org/abs/1605.06503))
- Poggianti B. M., et al., 2013, *ApJ*, **762**, 77
- Pozzetti L., et al., 2010, *A&A*, **523**, A13
- Quilis V., Trujillo I., 2013, *ApJ*, **773**, L8
- Reis R. R. R., et al., 2012, *ApJ*, **747**, 59
- Rosen S. R., et al., 2016, *A&A*, **590**, A1
- Ryan Jr. R. E., et al., 2012, *ApJ*, **749**, 53
- Rykoff E. S., et al., 2014, *ApJ*, **785**, 104
- Schaye J., et al., 2015, *MNRAS*, **446**, 521
- Schmidt M., 1968, *ApJ*, **151**, 393
- Shen S., Mo H. J., White S. D. M., Blanton M. R., Kauffmann G., Voges W., Brinkmann J., Csabai I., 2003, *MNRAS*, **343**, 978
- Somerville R. S., Davé R., 2015, *ARA&A*, **53**, 51
- Stoughton C., et al., 2002, *AJ*, **123**, 485
- Strateva I., et al., 2001, *AJ*, **122**, 1861
- Stringer M., Trujillo I., Dalla Vecchia C., Martínez-Valpuesta I., 2015, *MNRAS*, **449**, 2396
- Swetz D. S., et al., 2011, *ApJS*, **194**, 41
- Taylor E. N., Franx M., Glazebrook K., Brinchmann J., van der Wel A., van Dokkum P. G., 2010, *ApJ*, **720**, 723
- Timlin J. D., et al., 2016, *ApJS*, **225**, 1
- Toft S., et al., 2014, *ApJ*, **782**, 68
- Tortora C., et al., 2016, *MNRAS*, **457**, 2845
- Trujillo I., et al., 2006, *MNRAS*, **373**, L36
- Trujillo I., Cenarro A. J., de Lorenzo-Cáceres A., Vazdekis A., de la Rosa I. G., Cava A., 2009, *ApJ*, **692**, L118
- Trujillo I., Ferré-Mateu A., Balcells M., Vazdekis A., Sánchez-Blázquez P., 2014, *ApJ*, **780**, L20
- Valentinuzzi T., et al., 2010a, *ApJ*, **712**, 226
- Valentinuzzi T., et al., 2010b, *ApJ*, **721**, L19
- Viero M. P., et al., 2014, *ApJS*, **210**, 22
- Vogelsberger M., et al., 2014, *Nature*, **509**, 177
- Weiner B. J., et al., 2005, *ApJ*, **620**, 595
- Wellons S., et al., 2015, *MNRAS*, **449**, 361
- Wellons S., et al., 2016, *MNRAS*, **456**, 1030
- Whitaker K. E., et al., 2011, *ApJ*, **735**, 86
- Whitaker K. E., Kriek M., van Dokkum P. G., Bezanson R., Brammer G., Franx M., Labbé I., 2012, *ApJ*, **745**, 179
- Williams R. J., Quadri R. F., Franx M., van Dokkum P., Labbé I., 2009, *ApJ*, **691**, 1879
- Williams C. C., et al., 2015, *ApJ*, **800**, 21
- Woo J., Dekel A., Faber S. M., Koo D. C., 2015, *MNRAS*, **448**, 237
- Wright E. L., et al., 2010, *AJ*, **140**, 1868
- Wuyts S., et al., 2007, *ApJ*, **655**, 51
- York D. G., et al., 2000, *AJ*, **120**, 1579
- Zolotov A., et al., 2015, *MNRAS*, **450**, 2327
- Zu Y., Mandelbaum R., 2016, *MNRAS*, **457**, 4360
- de la Rosa I. G., La Barbera F., Ferreras I., Sánchez Almeida J., Dalla Vecchia C., Martínez-Valpuesta I., Stringer M., 2016, *MNRAS*, **457**, 1916
- van Dokkum P. G., et al., 2008, *ApJ*, **677**, L5
- van Dokkum P. G., et al., 2010, *ApJ*, **709**, 1018
- van Dokkum P. G., et al., 2015, *ApJ*, **813**, 23
- van der Wel A., et al., 2014, *ApJ*, **788**, 28

This paper has been typeset from a \LaTeX file prepared by the author.